Chinese Chemical Letters 36 (2025) 109942

Contents lists available at ScienceDirect

Chinese Chemical Letters

journal homepage: www.elsevier.com/locate/cclet

Construction of biomimetic hybrid nanovesicles based on M1 macrophage-derived exosomes for therapy of cancer

Yunyan Li[a], Zimin Cai[a], Zhicheng Wang[a], Sifeng Zhu[a], Wendian Liu[a], Cheng Wang[a,b,*]

[a] Key Laboratory of Marine Drugs, Chinese Ministry of Education, School of Medicine and Pharmacy, Ocean University of China, Qingdao 266003, China
[b] Laboratory for Marine Drugs and Bioproducts, Pilot National Laboratory for Marine Science and Technology, Qingdao 266237, China

ARTICLE INFO

Article history:
Received 20 February 2024
Revised 24 April 2024
Accepted 28 April 2024
Available online 29 April 2024

Keywords:
Tumor-associated macrophages
M1-Exos
Hybrid nanovesicles
Immunogenic cell death
Immunochemotherapy

ABSTRACT

Established evidence has unveiled two strategies for treating cancer: depleting tumor-associated macrophages (TAMs) and reprogramming M2-like TAMs into an antitumor M1 phenotype. Here, we designed novel pH-sensitive biomimetic hybrid nanovesicles (EDHPA) loaded with doxorubicin (DOX). DOX@EDHPA can specifically target TAMs by activating macrophage-derived exosomes (M1-Exos) and anisamide (AA) as cancer-specific targeting ligands. *In vitro* and *in vivo* studies demonstrated that DOX@EDHPA could efficiently be delivered to the tumor site and taken up by cells. Meanwhile, it synergistically enhanced immunogenic cell death (ICD) and induced a subsequent antigen-specific T cell immune response. The tumor inhibitory rate of the DOX@EDHPA group was 1.42 times that of the free DOX group. Further analysis showed that the excellent antitumor effects of DOX@EDHPA should ascribe to the homing effect of M1-Exos on macrophages and the repolarization to antitumor M1 TAMs, which induced the elevated secretion of pro-inflammatory factors. Therefore, the hybrid EDHPA targeting TAMs to reshape the tumor microenvironment constituted a novel immunochemotherapy strategy to inhibit tumor growth.

Immunochemotherapy has garnered significant attention for its potential to enhance synergistic effects on tumor suppression [1,2]. Conventional chemotherapeutics have long been considered immunosuppressive or tolerogenic [3]. However, recent evidence suggests that specific chemotherapy regimens, including paclitaxel, oxaliplatin, and doxorubicin (DOX), can induce immunogenic cell death (ICD) [2,4]. This phenomenon leads to an improvement in tumor immunogenicity and regulation of the immunosuppressive tumor microenvironment. Integrating the ICD induced by chemotherapeutics with immunotherapy can potentiate the overall antitumor efficacy [5]. Unfortunately, chemotherapeutics compromise therapeutic efficacy because of their poor selectivity and off-target toxicity to normal tissues [6]. Therefore, developing a rational drug delivery platform for chemotherapeutics becomes critical.

Cell-derived exosomes (Exos) are 30–150 nm membrane-encased vesicles derived by virtually all cell types and identified in various body fluids [7-9]. Owing to Exos endogenous origin, low immunogenicity, target specificity, and biocompatibility, numerous research teams have investigated the therapeutic potential of Exos-mediated drug delivery [10,11]. In addition, the uptake of Exos by specific recipient tumor cells is mediated by exosomal surface proteins, which can control successful drug delivery and distribution [12]. All these features make Exos an ideal cell-free carrier for immunotherapy to induce an antitumor-immune response and prevent tumor growth [13].

Tumor-associated macrophages (TAMs) are the most abundant infiltrating immune cells in the tumor microenvironment (TME) and play an essential role in tumor progression [14]. Their phenotypes represent the two extremes of the broad range of macrophage functional states [15]. M1-like TAMs exhibit a pro-inflammatory and antitumor phenotype, characterized by the expression and production of high levels of pro-inflammatory cytokines. M2-like TAMs promote tumor progression and suppress immunity [16]. Previous studies have indicated that modification of a macrophage membrane provides nanoparticles with the potential for drug delivery in response to the TME [17]. Meanwhile, Exos secreted from M1 macrophages induce repolarization of M2-like TAMs to M1 macrophages for tumor suppression [18], then stimulate the release of cytokines, such as tumor necrosis factor-α (TNF-α), interleukin-6 (IL-6), and IL-12, which cause activation of naive recipient immune cells [19].

Moreover, signal regulatory protein α (SIRPα)-CD47 is a critical signaling pathway in regulating immune cell responses [20].

* Corresponding author.
E-mail address: cheng13980029671@163.com (C. Wang).

https://doi.org/10.1016/j.cclet.2024.109942
1001-8417/

CD47 is overexpressed on the surface of tumor cells, interacting with SIRPα presented on macrophages, which protects tumor cells from phagocytosis by macrophages by sending "don't eat me" signal [21,22]. Recent advances have revealed that the SIRPα protein on the surface of M1-type macrophage Exos can interrupt the binding of CD47 on the surface of tumor cells to SIRPα on the surface of macrophages, thereby effectively activating phagocytosis of tumor cells by macrophages and downstream antitumor immune responses [23].

However, the isolation of Exos in the quantities needed for application is limited due to its poor yield [24-26], surface functionalization complexity, and size heterogeneity [27]. Owing to the low colloidal stability and low drug-loading efficiency, Exos with different therapeutics remains a primary challenge. Therefore, optimizing the Exos-based drug delivery system is a critical issue. Recently, based on the similar lipid bilayer of Exos and liposomes, a great emphasis has been placed on hybrid nanovesicles *via* fusing liposomes with Exos [28-30]. More importantly, hybrid nanovesicles *via* fusing immunogenic vesicles with liposomes to encapsulate chemotherapeutics are a potential approach for effective immunochemotherapy [31].

Herein, we designed pH-responsive, biomimetic hybrid nanovesicles (EDHPA), which was fabricated by efficient fusion of M1-Exos with pH-sensitive liposomes (Scheme 1A) for both tumor-targeted delivery and tumor-triggered release of the chemotherapeutic DOX (DOX@EDHPA). The pH-sensitive liposomes (DHPA) are connected with a target anisamide (AA), a low-molecular-weight benzamide derivative used as a tumor-directing moiety in functionalized nanosystems, based on its alleged interaction with sigma receptors [32]. We simultaneously prepared ordinary liposomes (DP) to compare liposome targeting and pH responsiveness. M1-Exos could repolarize M2-like TAMs to M1-like TAMs and be subsequently used to potentiate the anticancer efficiency. Moreover, the preserved macrophage surface proteins SIRPα in DOX@EDHPA could competitively bind with the CD47 surface receptor on tumor cells, effectively interrupting the generation of the "don't eat me" signal and increasing the phagocytosis of macrophages to tumor cells (Scheme 1B). Thus, DOX@EDHPA showed significant superiority antitumor activity in the mice cancer model. The hybrid nanovesicles will be a promising platform for synergistic immunochemotherapy and the development of enhanced drug delivery.

To prepare the nanovesicles, we first obtained polarized M1 macrophages. The purity of polarized RAW264.7 cells was quantified using flow cytometric analysis; a 64.2% ratio of RAW264.7 cells was successfully activated to be M1 phenotype (Fig. S1 in Supporting information). M1-Exos was first collected and characterized using previously reported methods (Fig. S2 in Supporting information) [33]. The size of exosomes was found to be 101.0 ± 2.6 nm. Transmission electron microscope (TEM) displayed that the exosomes presented a typical cup-shaped morphology. More importantly, Western blot assay showed that the exosomes express membrane protein and specific protein markers of macrophage SIRPα [34]. According to the above experimental results, the exosomes derived from M1 macrophages were successfully extracted by ultracentrifugation.

Then, we use 1,2-distearoyl-*sn*-glycero-3-phosphoethanolamine-*N*-[methoxy(polyethylene glycol)−2000 (DSPE-PEG$_{2000}$) or DSPE-Hyd-PEG$_{2000}$-AA to obtain DP, DHPA, and EDHPA. The morphologies, size distribution, and surface zeta potential of nanovesicles were characterized using dynamic light scattering (DLS, Fig. 1A). The size of EDHPA was around 122.4 ± 0.608 nm (polymer dispersity index (PDI), 0.167 ± 0.007), while M1-Exos and DHPA were 167.0 ± 1.206 nm (PDI, 0.200 ± 0.008) and 98.15 ± 0.239 nm (PDI, 0.201 ± 0.011). The size of DP was around 96.74 ± 1.304 nm (PDI, 0.217 ± 0.018). All nanovesicles showed better size homogeneity. In addition, there was a decreased zeta potential of EDHPA (-18.53 ± 0.611 mV) compared with DHPA (-15.57 ± 0.851 mV), probably due to the insertion of M1-Exos membrane lipids (-33.43 ± 2.108 mV). The TEM indicated that all samples displayed characteristics of nearly spherical vesicles (Fig. 1B). The nanoscale size can benefit the substantial accumulation of EDHPA into the tumor *via* the enhanced permeability and retention (EPR) effect [35].

The remote loading method was utilized to obtain DOX-loaded nanovesicles. The drug encapsulation efficiency (EE) and loading capability (LC) of different DOX-loaded nanovesicles

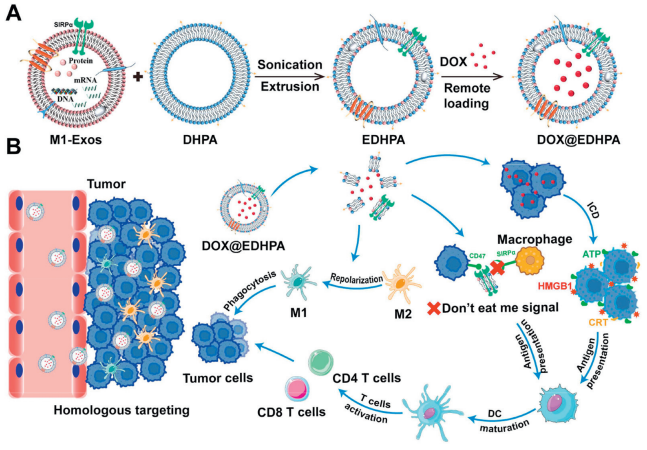

Scheme 1. (A) Preparation of DOX@EDHPA by the cofusion of M1-Exos with artificial liposomes. (B) Mechanism of immunochemotherapy based on the DOX@EDHPA for tumor suppression.

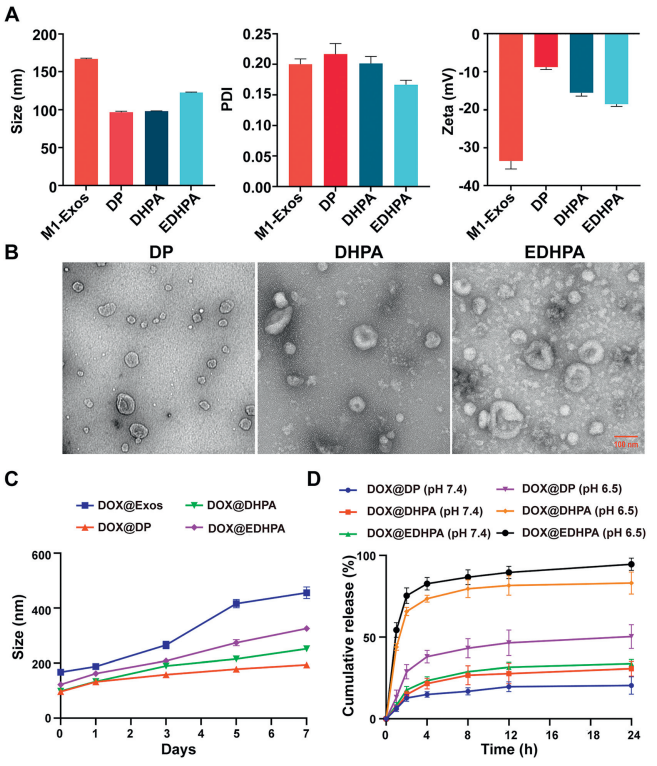

Fig. 1. (A) Hydrodynamic size distribution and zeta potential of M1-Exos, DP, DHPA, and EDHPA. (B) TEM of DP, DHPA, and EDHPA. Scale bar: 100 nm. (C) Stability of nanovesicles over the period in terms of size change at 4 °C. (D) Cumulative release of DOX@DP, DOX@DHPA, and DOX@EDHPA in different release media. Data are presented as mean ± standard deviation (SD) ($n = 3$).

were calculated (Table S1 in Supporting information). DOX@DP and DOX@DHPA showed a similar drug loading effect with DOX@EDHPA, indicating that the insertion of the Exos membrane had no significant effect on drug loading efficiency. In contrast, the EE and LC of Exos were much lower, EE was below 50%, and LC was below 5%. The colloidal stability was further evaluated by monitoring the particle size for one week. DOX@DP, DOX@DHPA and DOX@EDHPA remained stable for up to one week in biologically relevant solutions. At the same time, the particle size of DOX@Exos changed from 186 nm to 480 nm (Fig. 1C). The results indicated that fusing Exos with synthetic liposomes favored the structural stability of Exos. Due to the instability and low drug loading rate of Exos, we focused on the other groups in the following studies.

The drug release kinetics was further evaluated at physiological conditions (pH 7.4, phosphate buffered saline (PBS)) and in the acidic tumor microenvironment (pH 6.5, PBS). As exhibited in Fig. 1D, all drug-loaded nanovesicles released a small amount at pH 7.4 but increased at pH 6.5. This demonstrated that DOX@DHPA and DOX@EDHPA were stable at normal physiological pH (pH 7.4) but sensitive to the weak acidic tumor microenvironment. The pH-triggered release characteristic was attributed to the hydrazone bonds in lipid synthetic materials and increased solubility of DOX under acidic conditions. This feature ensures the release of DOX in the acidic tumor microenvironment.

We validated the cofusion of DHPA and M1-Exos. After fusing fluorescein isothiocyanate (FITC)-labeled liposomes with exosomes, 97.4% of nanovesicles were FITC-positive in the EDHPA by nanometer flow cytometry (Nano FCM, Fig. S3 in Supporting information). DHPA-DiO and M1-Exos-DiI scattered green and red fluorescence separately when just mixed physically. While undergoing hydration and serial extrusions, the red and green fluorescence in EDHPA was merged entirely (Fig. S4 in Supporting information). Furthermore, Fourier transform infrared spectroscopy (FTIR) was carried out to identify the vibrational modes and chemical characteristics of M1-Exos, DHPA, and EDHPA. It shows specific absorption bands of the FTIR spectrum of EDHPA, the characteristic bands of M1-Exos at about 3500 cm^{-1}, and the characteristic bands of DHPA at 3000 cm^{-1} (Fig. S5 in Supporting information). The above results confirmed the successful formation of EDHPA.

Phagocytosis of tumor cells is a crucial step for macrophage-mediated presentation of tumor cell antigens [23]. To verify the expression of SIRP, EDHPA and CD47 pre-saturated EDHPA were incubated with tumor cells, respectively, and CD47-FITC antibody coupled to the probe was added. The results showed that EDHPA could bind to CD47 on the surface of tumor cells after incubation with tumor cells, making the anti-CD47-FITC unable to bind to them. The SIRPα on the surface of EDHPA pre-saturated with CD47 protein is saturated, making the CD47 on the surface of tumor cells unable to bind to it and bind to the probe (Fig. S6 in Supporting information). It proved the SIRPα expression on the EDHPA surface, and it could bind to CD47 on the surface of tumor cells. After that, M1 macrophages and tumor cells 4T1 were co-cultured with EDHPA and CD47 pre-saturated EDHPA. According to the results (Fig. S7 in Supporting information), EDHPA could significantly enhance the phagocytosis of tumor cells by macrophages. These results suggest that EDHPA promoted phagocytosis through competitive interaction with CD47 on the surface of cancer cells.

The *in vitro* cytotoxicity of the nanovesicles was evaluated and compared to free DOX using cell counting kit-8 (CCK8) assays. According to the results, DOX@EDHPA efficiently inhibited cell proliferation compared with DOX@DHPA (Fig. 2A). However, no significant inhibition effects were observed in the blank EDHPA-treated group. It demonstrated the security of EDHPA. It was found that all treatment groups showed dose-dependent cytotoxicity (Fig. 2B). Compared with the free DOX (half maximal inhibitory concentration $IC_{50} = 1.646$ μg/mL), the antiproliferative effects on 4T1 cells

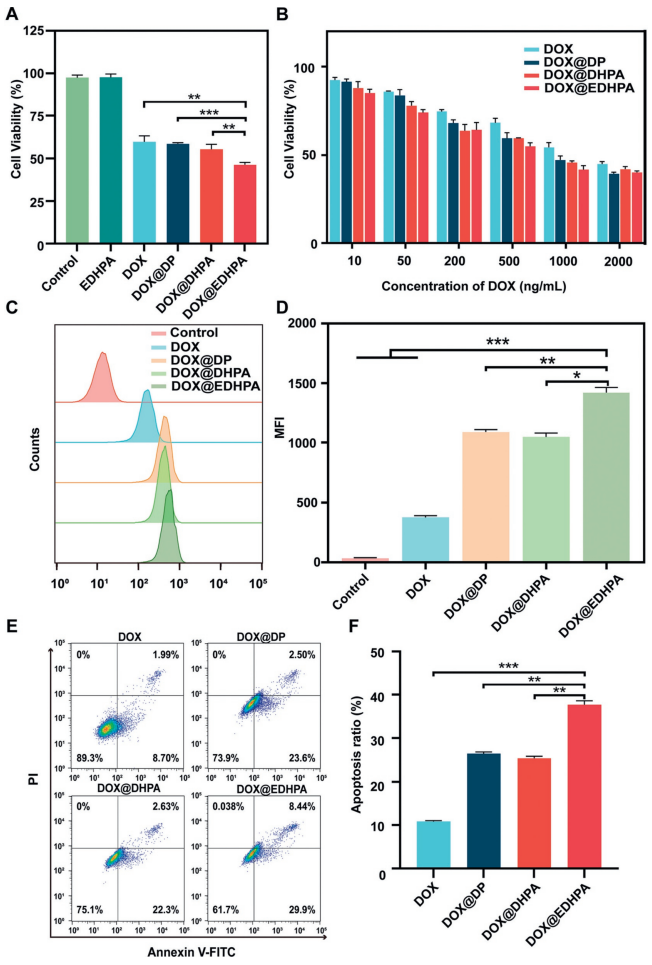

Fig. 2. The antitumor effects of DOX-loaded formulations *in vitro*. Viability of 4T1 cells after incubating 24 h at the same DOX concentrations (A) and different DOX concentrations (B) with different formulations. (C) The cellular uptake after treatment with different DOX-loaded formulations and (D) the mean fluorescence intensity (MFI) values of the data shown in (C). (E) Apoptotic cell proportions after treatment with different DOX-loaded formulations. (F) Percentage of apoptotic cells in (E). Data are presented as mean ± SD ($n = 3$). $^{***}P < 0.001$, $^{**}P < 0.01$, $^{*}P < 0.05$.

of DOX@DP ($IC_{50} = 0.907$ μg/mL), DOX@DHPA ($IC_{50} = 0.884$ μg/mL) and the DOX@EDHPA ($IC_{50} = 0.672$ μg/mL) all were better, of which DOX@EDHPA has the best effect.

To induce ICD in tumor cells, efficient cellular uptake of ICD inducers by tumor cells is critical. According to the result (Figs. 2C and D), the drug internalization of nanovesicals was higher than that in the free DOX group. In addition, the DOX@EDHPA group exhibited higher intracellular DOX amounts compared to the DOX@DHPA, indicating the M1-Exos with liposomes *via* membrane fusion facilitated the internalization of nanovesicles to accessible cells. The *in vitro* antitumor efficacy was also evaluated through Annexin V-FITC/propidium iodide (PI) apoptosis assay. Figs. 2E and F showed that the tumor cells treated with DOX@EDHPA depicted the most potent ability to induce apoptosis and exhibited a very significant difference in total apoptosis ratio with free DOX and other control treatments, which showed conformance with the results of cell viability assay.

It has been reported that exosome-mimetic nanovesicles derived from M1 macrophages could repolarize M2 TAMs to M1 macrophages that release pro-inflammatory cytokines and induce antitumor immune responses [18]. To investigate whether the EDHPA induces the release of inflammatory cytokines, we used enzyme-linked immunosorbent assay (ELISA) to determine the ex-

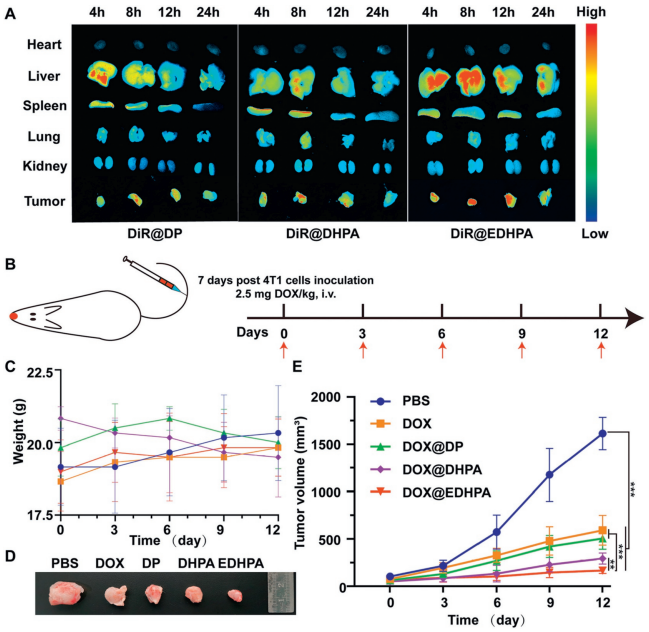

Fig. 3. (A) *Ex vivo* biodistribution of DiR@DP, DiR@DHPA, and DiR@EDHPA in tumors and main organs at different time intervals through IVIS. (B) Scheme depicting the BALB/c mice receiving the treatment on days 0, 3, 6, 9, and 12. (C) Weight change of 4T1 tumor-bearing mice injected with different therapies. (D) Photographs of 4T1 subcutaneous tumors at the end of treatment. (E) Tumor volume growth curves of 4T1 tumor-bearing mice injected with different therapies. Data are presented as mean ± SD ($n = 6$) $^{***}P < 0.001$, $^{**}P < 0.01$.

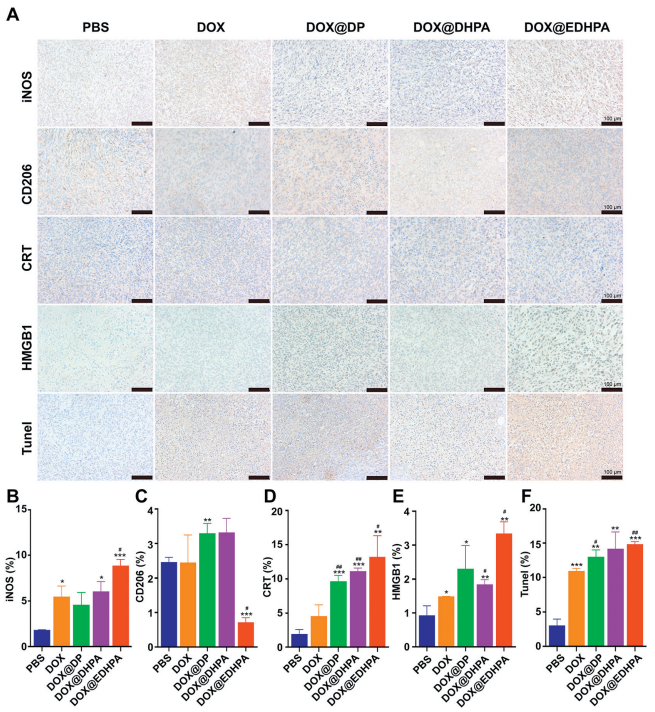

Fig. 4. Histological/biochemical analysis of tumor after treatment. (A) iNOS, CD206, CRT, HMGB1 and TUNEL staining of tumor sections. Scale bar: 100 μm. Detection of iNOS$^+$ cells (B), CD206$^+$ cells (C), CRT (D), HMGB1 (E) and TUNEL (F) in tumor sections. Data are shown as means ± SD ($n = 3$). $^{***}P < 0.001$, $^{**}P < 0.01$, $^{*}P < 0.05$ *vs.* the PBS group; $^{\#\#}P < 0.01$, $^{\#}P < 0.05$ *vs.* the DOX group.

pression level of pro-inflammatory cytokines in a co-culture system. The result showed that both M1-Exos and EDHPA could promote the expression of IL-6, IL-12 and TNF-α (Fig. S8 in Supporting information). It demonstrated that EDHPA can promote anti-tumor immune response *in vivo*.

We then developed animal tumor models *in vivo*. All animal studies were conducted in accordance with the guidelines of the Experimental Animal Ethics Committee of Ocean University of China (No. OUC-SMP-2023–07–02). To examine the *ex vivo* biodistribution of nanovesicles, we employed a 4T1 tumor-bearing mouse model. The tumor cells were administered subcutaneously (s.c.). The tumor and main organs were obtained and imaged at predetermined intervals under the IVIS Lumina XR system. Fig. 3A shows that accumulative fluorescence intensity in the tumor increased with prolonging time and reached the summit at 8–12 h after injection. The results indicated that nanovesicles could efficiently accumulate at the tumor site, probably attributed to the fact that the dynamic vascular vent in the tumor enhanced the permeability of tumor blood vessels and allowed the extravasation of nanovesicles into the cancer. Importantly, stronger fluorescence derived from DiR@EDHPA was observed during the whole period at the tumor site compared with DiR@DP and DiR@DHPA, showing that more EDHPA accumulated and retained in the tumor due to the specific targeting ability. The above results demonstrated that EDHPA had a tumor-targeting effect, benefiting the synergistic antitumor immune response.

Encouraged by the above results, we determined the antitumor effects of DOX@EDHPA treatment *in vivo*. The established 4T1 subcutaneous model mice were injected with PBS, DOX, DOX@DP, DOX@DHPA, and DOX@EDHPA (2.5 mg DOX/kg) on days 0, 3, 6, 9, 12 and sacrificed on day 13 (Fig. 3B). Chemotherapy is often associated with weight loss, which is a common side effect in treated mice. The potential toxicity of different formulations was assessed in BALB/c mice. Compared with the PBS-treated groups, mice in treatment groups did not show apparent weight loss (Fig. 3C), indicating that the treatments caused no overt toxicity. Fig. 3D was a graph of the tumor after 12 days of treatment in different groups. Fig. 3E showed the change in tumor volume with time. The tumor inhibitory rate was calculated according to the final tumor volume of each group (Table S2 in Supporting information). We found that compared with the PBS group, all other groups inhibited the growth of tumors to a certain degree. The development of tumors injected with free DOX solution was slightly inhibited. The low antitumor efficiency arises from its short retention in the blood and rapid clearance *in vivo*. Compared with the free DOX group, the DOX@DP group had a better tumor growth inhibition effect, which might be attributed to the fact that the encapsulation of lipids bilayers not only improved the chemical stability but also increased the DOX accumulation into the tumor through the EPR effect. The better antitumor impact of the DOX@DHPA group might be due to the AA target action and the hydrazone bond's acid response. Compared to all the groups mentioned above, DOX@EDHPA showed the strongest antitumor effect due to the fusion of the exosomes. More importantly, the expression of SIRPα on the surface of DOX@EDHPA prolonged the blood circulation time of nanovesicles by escaping immune recognition by mononuclear phagocytic system (MPS), achieving long retention *in vivo*.

The pathological changes of various organs were evaluated using the hematoxylin and eosin (H&E) staining assay to assess the safety of nanovesicles. As shown in Fig. S9 (Supporting information), compared with the control group, DOX@DP, DOX@DHPA, and DOX@EDHPA did not induce cell degeneration or necrosis in major organs, suggesting a reasonable safety margin in their application.

Paraffin sections of the tumors were used for immunohistochemistry (IHC) analysis of iNOS, CD206, calreticulin (CRT), high mobility group protein B1 (HMGB1), terminal deoxynucleotidyl transferase mediated dUTP nick end labeling (TUNEL) (Fig. 4A), CD4, and CD8. The polarized M1 macrophages could release pro-inflammatory cytokines, which induce antitumor immune re-

sponse. Briefly, iNOS is a marker of M1 macrophages, and CD206 is a marker of M2 macrophages. During DOX-induced ICD, CRT can be exposed to the surface of tumor cells, which helps to enhance the recognition and response of the immune system. At the same time, the up-regulation of CRT expression can also promote the release of HMGB1 into the microenvironment outside tumor cells [35]. As shown in Fig. 4, the DOX@EDHPA group showed a higher proportion of M1 macrophages compared to the PBS-treated groups (Fig. 4B) and a lower proportion of M2 macrophages compared to the PBS- and DOX-treated groups (Fig. 4C). Further demonstrating that EDHPA can efficiently eliminate M2-like TAMs and enhanced M1-like TAMs.

As immune cells in the tumor microenvironment play vital roles in tumor progression, it is crucial to understand the immunosuppressive tumor microenvironment's impact on immunotherapy's therapeutic efficacy. We further analyzed $CD4^+$ and $CD8^+$ T cell levels in tumor tissues (Fig. S10 in Supporting information). DOX@EDHPA significantly facilitated the recruitment of $CD4^+$ and $CD8^+$ T cells in tumors, especially the $CD8^+$ T cells. Figs. 4D and E showed that DOX@EDHPA significantly promoted CRT exposure and the release of HMGB1 compared to free DOX, DOX@DP, and DOX@DHPA. This may be attributed to the tumor's better accumulation and cellular uptake of DOX@EDHPA. Taken together, the EDHPA can deliver DOX to the tumor effectively for direct cytotoxicity and further initiate the ICD effect to improve the immunogenicity of the tumor. Meanwhile, the EDHPA with immunostimulatory activity can elicit an antigen-specific T-cell response for the synergistic antitumor effect. As shown in Fig. 4F, the number of apoptotic cells in the DOX@EDHPA group was significantly larger than those in the PBS- and DOX-treated groups, further demonstrating that repolarization of M2-like TAMs and retaining M1-like TAMs can significantly promote tumor immunotherapy.

To summarize, in this work, we have designed a specific targeting TAMs biomimetic nanovesicles based on the fusion of M1 macrophage-derived exosomes and pH-sensitive liposomes that synergistically enhanced immunochemotherapy. The preserved macrophage surface proteins SIRPα in EDHPA could competitively bind with the CD47 surface receptor on tumor cells, effectively interrupting the generation of the "don't eat me" signal. When the EDHPA was loaded with DOX, it could significantly promote CRT exposure and the release of HMGB1. Moreover, EDHPA could efficiently eliminate M2-like TAMs and enhance M1-like TAMs, facilitating the recruitment of $CD4^+$ and $CD8^+$ T cells in tumors. Overall, this work represents a significant advancement in establishing a drug delivery system through chemotherapy and immunotherapy. This study further proves that exosomes have broad application prospects as drug delivery carriers in treating tumors. Future studies can significantly improve the efficacy by designing appropriate exosome delivery systems while promoting exosome clinical application in tumor therapy.

Declaration of competing interest

The authors declare that they have no known competing financial interests or personal relationships that could have appeared to influence the work reported in this paper.

CRediT authorship contribution statement

Yunyan Li: Writing – original draft, Methodology, Formal analysis, Data curation, Conceptualization. **Zimin Cai:** Writing – review & editing, Software, Methodology, Formal analysis. **Zhicheng Wang:** Visualization, Methodology, Conceptualization. **Sifeng Zhu:** Writing – review & editing, Software. **Wendian Liu:** Formal analysis. **Cheng Wang:** Writing – review & editing, Supervision, Funding acquisition, Conceptualization.

Acknowledgment

This work was supported by the National Natural Science Foundation of China (No. NSFC31872754).

Supplementary materials

Supplementary material associated with this article can be found, in the online version, at doi:10.1016/j.cclet.2024.109942.

References

[1] S. Shen, H.J. Li, K.G. Chen, et al., Nano Lett. 17 (2017) 3822–3829.
[2] Y. Chen, R. Xia, Y. Huang, et al., Nat. Commun. 7 (2016) 13443.
[3] X. Duan, C. Chan, W. Han, et al., Nat. Commun. 10 (2019) 1899.
[4] A.M. Cook, W.J. Lesterhuis, A.K. Nowak, R.A. Lake, Curr. Opin. Immunol. 39 (2016) 23–29.
[5] T.A.P. Driedonks, S.G. van der Grein, Y. Ariyurek, et al., Cell. Mol. Life Sci. 75 (2018) 3857–3875.
[6] S. Quader, K. Kataoka, Mol. Ther. 25 (2017) 1501–1513.
[7] S. Kourembanas, Annu. Rev. Physiol. 77 (2015) 13–27.
[8] Y. Wu, Z. Zhang, Y. Wei, Z. Qian, X. Wei, Chin. Chem. Lett. 34 (2023) 108098.
[9] N.L. Syn, L.Z. Wang, E.K.H. Chow, C.T. Lim, B.C. Goh, Trends Biotechnol. 35 (2017) 665–676.
[10] J. Dai, Y. Su, S. Zhong, et al., Signal Transduct. Target Ther. 5 (2020) 145.
[11] Y. Zhang, Y. Liu, H. Liu, W.H. Tang, Cell Biosci. 9 (2019) 19.
[12] A. Mukherjee, B. Bisht, S. Dutta, M.K. Paul, Acta Pharmacol. Sin. 43 (2022) 2759–2776.
[13] H. Zhang, K. Tang, Y. Zhang, et al., Cancer Immunol. Res. 3 (2015) 196–205.
[14] F.O. Martinez, A. Sica, A. Mantovani, M. Locati, Front. Biosci. 13 (2008) 453–461.
[15] M. Yang, J.Q. Chen, F. Su, et al., Mol. Cancer 10 (2011) 117.
[16] C.B. Anders, T.M.W. Lawton, H.L. Smith, et al., J. Leukoc. Biol. 111 (2022) 667–693.
[17] T. Yin, Q. Fan, F. Hu, et al., Nano Lett. 22 (2022) 6606–6614.
[18] Y.W. Choo, M. Kang, H.Y. Kim, et al., ACS Nano 12 (2018) 8977–8993.
[19] J.A. Reales-Calderon, C. Vaz, L. Monteoliva, G. Molero, C. Gil, J. Proteome Res. 16 (2017) 87–105.
[20] L. Cheng, X. Zhang, J. Tang, Q. Lv, J. Liu, Biomaterials 275 (2021) 120964.
[21] R. Majeti, M.P. Chao, A.A. Alizadeh, et al., Cell 138 (2009) 286–299.
[22] A. Macedo-Pereira, C. Martins, J. Lima, B. Sarmento, J. Control. Release 358 (2023) 98–115.
[23] Q. Lv, L. Cheng, Y. Lu, et al., Adv. Sci. 7 (2020) 2000515.
[24] M.S. Kim, M.J. Haney, Y. Zhao, et al., Nanomedicine 14 (2018) 195–204.
[25] K.M. Kanninen, N. Bister, J. Koistinaho, T. Malm, Biochim. Biophys. Acta 1862 (2016) 403–410.
[26] S.M. van Dommelen, P. Vader, S. Lakhal, et al., J. Control. Release 161 (2012) 635–644.
[27] J. Gao, S. Wang, Z. Wang, Biomaterials 135 (2017) 62–73.
[28] M. Piffoux, A.K.A. Silva, C. Wilhelm, F. Gazeau, D. Tareste, ACS Nano 12 (2018) 6830–6842.
[29] W.J. Goh, S. Zou, C.K. Lee, et al., Biomacromolecules 19 (2018) 22–30.
[30] Y. Lin, J. Wu, W. Gu, et al., Adv. Sci. 5 (2018) 1700611.
[31] M. Hu, J. Zhang, L. Kong, et al., ACS Nano 15 (2021) 3123–3138.
[32] A. Dasargyri, C.D. Kümin, J.C. Leroux, Adv. Mater. 29 (2016) 1603451.
[33] J. Cho, Y.S. Lee, S.H. Kim, J.K. Ko, C.W. Kim, Cancer Lett. 275 (2009) 256–265.
[34] S. Rayamajhi, T.D.T. Nguyen, R. Marasini, S. Aryal, Acta Biomater. 94 (2019) 482–494.
[35] D. Kalyane, N. Raval, R. Maheshwari, et al., Mater. Sci. Eng. C Mater. Biol. Appl. 98 (2019) 1252–1276.